

RESEARCH ARTICLE OPEN ACCESS

Using Short Molecular Dynamics Simulations to Determine the Important Features of Interactions in Antibody–Protein Complexes

A. Clay Richard  | Robert J. Pantazes 

Department of Chemical Engineering, Auburn University, Auburn, Alabama, USA

Correspondence: Robert J. Pantazes (rjp0029@auburn.edu)**Received:** 9 July 2024 | **Revised:** 15 October 2024 | **Accepted:** 13 November 2024**Funding:** This work was supported by the NSF EPSCoR RII Track-2 Award 2119237.**Keywords:** antibodies | antigens | binding proteins | molecular dynamics simulation | protein binding

ABSTRACT

The last few years have seen the rapid proliferation of machine learning methods to design binding proteins. Although these methods have shown large increases in experimental success rates compared to prior approaches, the majority of their predictions fail when they are experimentally tested. It is evident that computational methods still struggle to distinguish the features of real protein binding interfaces from false predictions. Short molecular dynamics simulations of 20 antibody–protein complexes were conducted to identify features of interactions that should occur in binding interfaces. Intermolecular salt bridges, hydrogen bonds, and hydrophobic interactions were evaluated for their persistences, energies, and stabilities during the simulations. It was found that only the hydrogen bonds where both residues are stabilized in the bound complex are expected to persist and meaningfully contribute to binding between the proteins. In contrast, stabilization was not a requirement for salt bridges and hydrophobic interactions to persist. Still, interactions where both residues are stabilized in the bound complex persist significantly longer and have significantly stronger energies than other interactions. Two hundred and twenty real antibody–protein complexes and 8194 decoy complexes were used to train and test a random forest classifier using the features of expected persistent interactions identified in this study and the macromolecular features of interaction energy (IE), buried surface area (BSA), IE/BSA, and shape complementarity. It was compared to a classifier trained only on the expected persistent interaction features and another trained only on the macromolecular features. Inclusion of the expected persistent interaction features reduced the false positive rate of the classifier by two- to five-fold across a range of true positive classification rates.

1 | Introduction

Recent years have seen a veritable explosion in the publication of machine learning (ML) protein design methods [1–4], including for binding proteins [5, 6]. This is a natural progression after the great successes that ML models had for the protein structure prediction problem, starting with AlphaFold2 [7] and RoseTTAFold [8]. While ML-based methods can correctly predict the structures of most proteins, the majority of ML-designed binders fail when experimentally tested. The highest experimental success

rate of such methods that the authors are aware of is 19% as reported for RFdiffusion [5]. While this is an orders of magnitude improvement over prior approaches, it is evident that such methods still predict an abundance of false positive complexes and that computational tools still struggle to distinguish the features of real protein–protein binding complexes from false ones [9–15].

A commonality of both AlphaFold2 and RoseTTAFold is that one of the features their algorithms consider is residue–residue

This is an open access article under the terms of the [Creative Commons Attribution-NonCommercial License](#), which permits use, distribution and reproduction in any medium, provided the original work is properly cited and is not used for commercial purposes.

© 2024 The Author(s). *PROTEINS: Structure, Function, and Bioinformatics* published by Wiley Periodicals LLC.

distance information (i.e., protein contact maps). Although ESMFold [16] has demonstrated that protein structures can be accurately predicted based on sequence information alone, AlphaFold2 and RoseTTAFold have shown that residue–residue interaction information can contribute to accurate ML protein prediction algorithms. Thus, considering how amino acids interact in protein interfaces is likely important to the successful design of binding proteins.

Prior literature has identified common features of protein binding interfaces, including the importance of prestabilized hotspot residues [17–25]. Hotspot residues are those that contribute a disproportionately large percentage of a complex's binding energy and are prestabilized when they have limited degrees of freedom prior to binding. Our own work has demonstrated outcomes relevant to this problem: that consideration of interaction properties rather than amino acid identities improves computational predictions [26]; that the effects of mutations in antibody–protein interfaces differ from their effects on protein structures [27]; and that consideration of prestabilization information for pairwise interactions in protein binding interfaces can improve the experimental success rate of ML-designed protein binders [28]. Considering all of these observations, we hypothesized that there are stability-related properties of interactions at protein–protein interfaces that can help computational methods eliminate false complexes from consideration.

Antibodies are the archetypical binding proteins. There is a known directionality to their binding (i.e., antibodies evolve to bind to antigens) and the properties of their structures and modes of binding have been extensively studied due to their importance in medicine and widespread use in experimental protocols. Specifically, antibodies bind using six modular loops known as complementarity determining regions (CDRs), with three in each of the two variable domains that compose their binding sites [29]. The understanding of these properties allowed for several experimentally validated algorithms specifically for designing antibodies to be developed [30–34]. Antibodies are a promising system to study for features of interactions that are important to protein binding because interactions in affinity matured antibody interfaces are unambiguously part of a complex evolved for maximum affinity.

Molecular dynamics (MD) simulations have been used to study many protein complexes over varying time scales [35–49]. Although it is common practice to assess the accuracy of computationally predicted protein complexes by comparing them to experimentally determined structures [12, 13, 15], it is possible that important features of interactions might only be revealed through study of their dynamic behaviors. In this study, short, 5 ns MD simulations of 20 antibody–protein complexes were conducted to study their behavior around the local minima of their experimental structures and to identify important features of the binding interfaces.

2 | Methods

Figure 1 is a schematic of the workflow used to conduct the analysis in this study. It began with selecting antibody–protein

complexes and running them through short MD simulations in triplicate. Geometric definitions from prior literature of salt bridges, hydrogen bonds, hydrophobic interactions, and residue stabilization were applied to the experimental structures as well as snapshots of their conformations from throughout the simulations. This led to the identification of expected persistent interactions that are present in the experimental structures and lasted throughout the simulations. Including the features of these interactions to train random forest classifiers resulted in a 2–5 fold reduction in false positive predictions.

2.1 | Antibody Selection

Twenty single-chain variable fragment (scFv) antibody–protein complexes were selected for analysis in this work. They were chosen on the basis of having experimentally determined structures in the Research Collaboratory for Structural Bioinformatics Protein Data Bank (RCSB PDB) ([RRID:SCR_012820](#)) [50], being a scFv, binding a protein antigen, and having no non-amino acid chemical groups in either the antibody or antigen. These criteria were applied so that the MD simulations were of the experimental structure and to limit the analysis to amino acid–amino acid interactions without allowing other chemical groups. In cases where parts of the antibody and/or antigen were not experimentally resolved, the missing pieces were predicted using RoseTTAFold ([RRID:SCR_018805](#)). Specifically, the entire structure of the protein with missing residues was predicted and then the missing portions were spliced into the experimental structures. This process allows for the atoms that were present in the crystal structure to be retained while creating a full atomistic representation of the protein for the simulations.

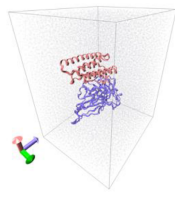
2.2 | Molecular Simulations and Macromolecular Features Calculations

Prior to MD simulation, a Chemistry at Harvard Macromolecular Mechanics (CHARMM) ([RRID:SCR_014892](#)) [51, 52] energy minimization was used to correct computationally perceived clashes in the experimental structures and to rectify any minor errors arising from the splicing process. The bond, angle, Urey–Bradley, dihedral angle, improper dihedral angle, electrostatic, and van der Waals (vdW) energy terms were used along with a harmonic force constant of $10 \frac{\text{kcal}}{\text{mol} \cdot \text{\AA}^2}$ on the N, C α , and C backbone atoms.

The MD simulation files were prepared using the QwikMD extension within Visual Molecular Dynamics (VMD) ([RRID:SCR_001820](#)) [53, 54]. The simulations were solvated using the TIP3P water model [55] with a 20 Å buffer. Chlorine and sodium ions were added such that the salt concentration was 0.15 mol/L. Simulations used the NpT ensemble and the CHARMM36 force field [56, 57] and were performed using the Nanoscale Molecular Dynamics (NAMD) ([RRID:SCR_014894](#)) simulation software [58]. Each simulation consisted of a 0.004 ns minimization stage, a 0.240 ns annealing stage that ramped the temperature from 60 to 300 K while maintaining pressure at 1 atm, a 5.000 ns equilibration stage at constant temperature and pressure, and a 5.000 ns

Antibody Selection and MD Simulation

20 scFv experimental structures selected from the PDB
Energy minimization of crystal structures
Short MD simulations run for each



Features of Pairwise Intermolecular Interactions

Origin

- Crystal Structure
- Simulation Only

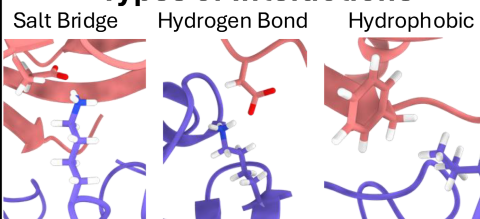
Type

- Salt Bridge
- Hydrogen Bond
- Hydrophobic

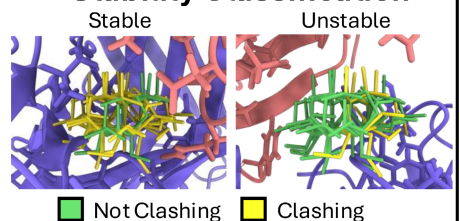
Stability

- No Stable Residues
- One Stable Residue
- Both Stable Residues

Types of Interactions



Stability Classification



Not Clashing Clashing

Expected Persistent Pairwise Interactions

Origin

- Crystal Structure ✓
- Simulation Only ✗

Stable Residues

	None	One	Both
Salt bridge	✓	✓	✓
Hydrogen Bond	✗	✗	✓
Hydrophobic Interaction	✓	✓	✓

Discriminating False Poses Using Pairwise Features

Two Random Forest Classifiers

Macromolecular Features Only

Including Expected Persistent Pairwise Interactions



vs.



Two to Five-Fold Improvement in False Positive Rate

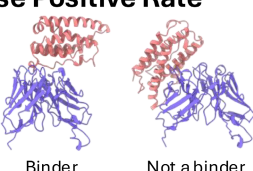


FIGURE 1 | Schematic of the workflow used in this study. Twenty antibody-protein complexes were selected for study and analyzed with MD simulations. The properties of their pairwise residue interactions were evaluated, leading to the identification of expected persistent interactions that are present in experimental structures and last throughout the simulations. These properties were used as features in a random forest classifier, resulting in a 2–5 reduction in false positive classifications.

production stage also at constant temperature and pressure. Pressure was maintained using the Nosé-Hoover Langevin Piston while Langevin dynamics was used when temperature was held constant [59, 60]. Per standard practice, backbone atoms were fixed during the annealing and equilibration stages. Structures from 500 evenly spaced time points (0.01 ns apart) were kept for analysis. Simulations were repeated in triplicate for each of the 20 scFv complexes (i.e., 60 total simulations). Calculations were performed using a standard node

on Auburn University's Easley High Performance Computing cluster consisting of 48 Intel Xeon Gold 6248R processors with 192 GB of RAM.

Five macromolecular features were calculated for each of the 500 structures from each simulated trajectory: root mean square displacement (RMSD) from the energy-minimized crystal structure, interaction energy (IE), buried surface area (BSA), IE per BSA (IE/BSA), and shape complementarity (SC).

These features describe properties of the bound complex as a whole, instead of properties of pairs of interacting amino acids. RMSD was calculated using all atoms after superimposing the structures using the Kabsch algorithm [61, 62]. IE, BSA, IE/BSA, and SC were calculated using Rosetta's ([RRID:SCR_015701](#)) *InterfaceAnalyzer* protocol [63]. The standard deviations of these macromolecular features during each simulation trajectory were calculated.

2.3 | Pairwise Intermolecular Interactions

This work considered three types of interactions between amino acids at the binding interface: salt bridges, hydrogen bonds, and hydrophobic interactions. As in a previous work [28], the interactions were defined using geometric criteria. Salt bridges consisted of atoms of opposite charge (e.g., the charged N and O in lysine and aspartic acid, respectively) within 4 Å of each other [64]. Hydrogen bonds were defined as polar hydrogens and acceptor atoms within 2.5 Å of one another with the donor-hydrogen-acceptor (DHA) angle being greater than 120° and the donor-acceptor-antecedent (DAA) angle being at least 90° [65]. Finally, hydrophobic interactions were those that buried at least 24.438 Å² of nonpolar surface area [28]. This definition of hydrophobic interactions is inclusive of pi-pi interactions.

Pi-cation interactions were considered for inclusion in this study but were found to be exceedingly rare. They were defined as a positively charged atom within 6 Å of the center of mass of an aromatic ring with an angle of not more than 15° between the vector from the center of the ring to the positively charged atom and the normal vector of the aromatic plane [66]. Only one such interaction was found in the 20 scFv structures analyzed in this study. As one interaction is too few to draw statistically meaningful conclusions, pi-cation interactions were not analyzed further.

Interface residues were defined as those within 6 Å of a residue on the other protein [67]. Every possible residue-residue pair in the interface was classified as either non-interacting or as forming a salt bridge, hydrogen bond, or hydrophobic interaction. These classifications were separately applied to the CHARMM-minimized crystal structures and each of the 500 structures produced by each simulation. When a residue pair met multiple geometric criteria, they were classified as the rarest of the interaction types for which they qualified to avoid double counting the interactions in the analyses. Rarity was determined based on the number of times the interactions were identified in the energy minimized crystal structures, with salt bridges being the rarest interaction type, followed by hydrogen bonds, and then hydrophobic interactions. This order also corresponds to the observed average strengths of the interactions, with salt bridges being stronger than hydrogen bonds and hydrophobic interactions being the weakest interaction type. Thus, it was considered likely that the energies of interactions that met multiple geometric criteria were dominated by the rarest (i.e., strongest) interaction type.

The persistence of an interaction was then defined as the fraction of the 500 structures from the MD simulation in which that geometric criterion was met. Intermolecular residue-residue interaction energies were calculated with the Residue Energy Breakdown protocol of Rosetta using the REF2015

parameterization [68]. Significance tests for interaction persistences and energies were performed using the Mann-Whitney U test [69] in the SciPy ([RRID:SCR_008058](#)) Stats package [70] (scipy.stats.mannwhitneyu). This test was used because it does not require assumptions about the expected distributions of the values, which are unknown for these properties.

Like the geometric criteria for interactions, definitions of amino acid stabilities from previous work were used [28]. Each residue was divided into two parts: backbone and side chain. Backbones were always considered to be stable because it was assumed that the covalent bonds with neighboring residues adequately limit their degrees of freedom. To assess the stability of the side chains, rotational isomers (i.e., rotamers) from the Dunbrack Rotamer Library [71] were aligned to the residue's position by aligning the nitrogen, α -carbon and β -carbon atoms. Side chains were classified as stable if they met any of several criteria. Charged side chains were stable if they formed two or more salt bridges. All side chains, including those with charges, were stable if more than 80% of their rotamers had at least one steric clash, defined as two non-hydrogen atoms being closer than 90% of the sum of their vdW radii. There were five exceptions to this 80% threshold. The first three were for glycine, alanine, and proline, which each only have a single side chain conformation and thus were always considered stable. The other two exceptions were for serine and threonine, which have three rotamers each and were considered stable if at least two of the three rotamers had steric clashes. Figure 2 shows an example of the stabilization criteria involving two lysine rotamer substitutions, one which resulted in a stable classification in the bound complex and one that was unstable.

Residue stabilities were determined from the energy minimized crystal structures. Each residue part was associated with two stabilization classifications: prestabilization and bound stabilization. The prestabilization label, stable or unstable, represents the degrees of freedom available in the free protein based only on intraprotein contacts. The bound stabilization label evaluates the same set of rotamers for clashes in the bound complex (i.e., intraprotein and interprotein residue neighbors are compared). A residue part can be unstable in the free protein and stable in the bound complex if its flexibility is restricted upon binding. Any residue part that is stable in the free protein, however, will be stable in the bound complex because the set of neighboring residues in the free protein is a subset of the neighboring residues in the bound complex. Whether a residue is stabilized is a binary decision, so the binomial distribution as implemented in the SciPy Stats package (scipy.stats.binomtest) was used to evaluate the statistical significance of residue stabilizations.

2.4 | Discriminating False Poses Using the Pairwise Features

The 20 scFv complexes were docked using ClusPro ([RRID:SCR_018248](#)) [72], HADDOCK ([RRID:SCR_019091](#)) [73], and RosettaDock ([RRID:SCR_013393](#)) [74]. Per the RosettaDock recommended protocol, the ZDOCK Server ([RRID:SCR_022518](#)) [75] was first used to perform global docking, and then RosettaDock was used to locally refine those

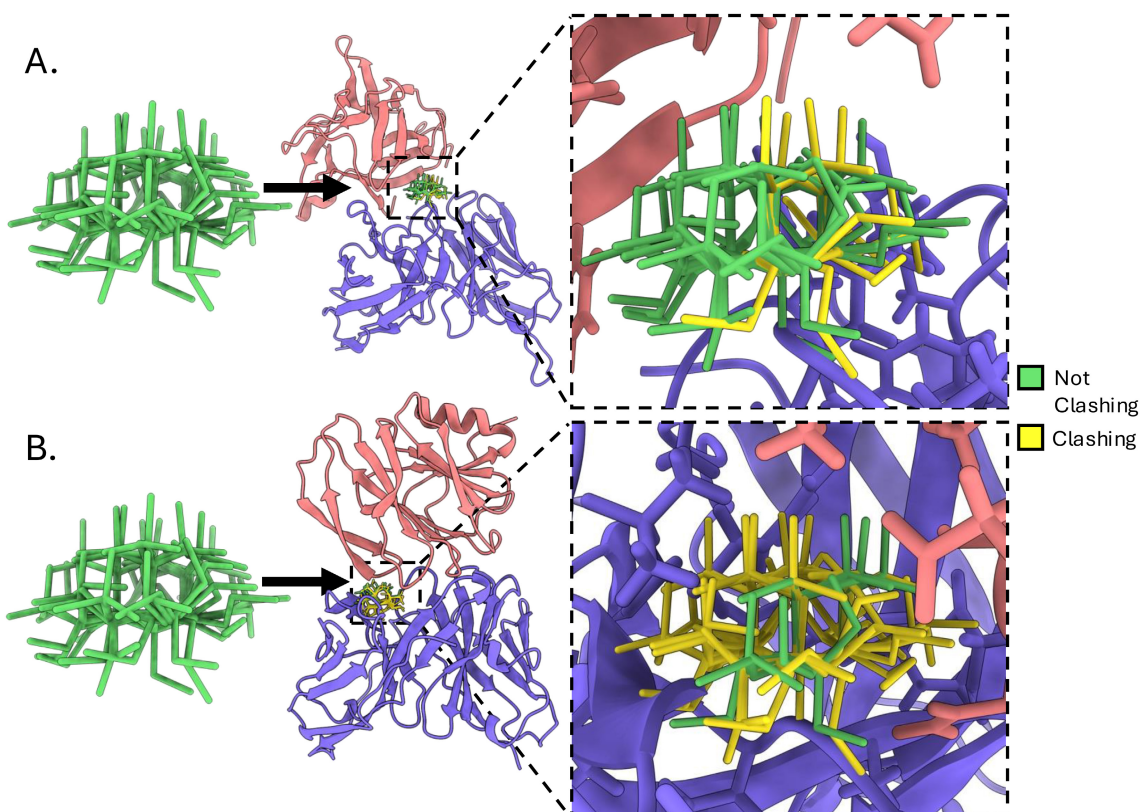


FIGURE 2 | Bound-stabilization of residues. Yellow and green represent clashing and nonclashing rotamers, respectively. Panel (A) depicts a lysine residue that is bound-unstable because most of its rotamer conformations do not have clashes while panel (B) shows a lysine residue that is bound-stable because most of its rotamer conformations have steric clashes.

predictions. ClusPro, HADDOCK, and ZDOCK all performed rigid body docking on the antibody and antigen structures, but HADDOCK also implemented a local refinement using a simulated annealing stage similar to RosettaDock's local refinement of the ZDOCK predictions. Complexes with infeasible binding modes (e.g., antigens predicted to be far from the antibody CDRs) were eliminated from consideration. Predicted complexes with an antigen RMSD > 10 Å were defined as poorly docked, a threshold and classification based on the DockQ score used in the Critical Assessment of PRediction of Interactions (CAPRI) [76]. Predicted complexes with an antigen RMSD ≤ 10 Å were collectively defined as acceptably docked, with subcategorizations of RMSDs ≤ 3, 5, and 10 Å. The docked complexes were minimized using CHARMM as previously described, then further refined using an all-atom energy minimization in Rosetta. Their interface residue–residue interaction classifications and stabilities were calculated as described.

The docked complexes were compared to the experimentally determined structures of 220 naturally occurring antibodies, which included the 20 scFv complexes analyzed with MD simulations. Experimentally unresolved portions of their structures were computationally predicted using the same protocol as for the complexes simulated with MD. The naturally occurring complexes were then minimized and had their pairwise interaction properties calculated in the same manner as the docked complexes.

A Scikit-learn ([RRID:SCR_019053](#)) random forest classifier (RandomForestClassifier) with default hyperparameters was

trained on the features of the poorly docked structures and the naturally occurring complexes [77]. The data were randomly split into training and test sets of 75% and 25%, respectively, such that each set contained equal ratios of poorly docked to naturally occurring complexes (i.e., stratified). This process was repeated 50 times, and the results were averaged. To evaluate the classification improvements provided by the pairwise interaction features, two identical protocols were performed: one using only the macromolecular features of IE, BSA, IE/BSA, and SC and the other using only the expected persistent pairwise interaction features. For further assessment and in addition to separating the data into stratified groups of 75% and 25% and repeating the classifier training 50 times, three sets of leave-one-out cross-validation (LOOCV) were also conducted: once using all features, once using only the four macromolecular features, and once using only the expected persistent pairwise interaction features. Finally, a classifier was trained using all features of the poorly docked and naturally occurring complexes and tested on the acceptably docked complexes to evaluate the effects of improving antigen RMSD.

3 | Results and Discussion

3.1 | Antibody Selection

Table S1 lists the PDB accession codes of the 20 complexes selected for analysis in this work, the number of amino acids in their antigens, and the portions of each structure that were

computationally predicted. Unsurprisingly, only one of the 20 complexes had an experimentally resolved linker between the variable domains in the scFv. The 220 antibody–protein complexes used for training and testing the random forest classifiers are listed in Table S2.

3.2 | Molecular Simulations and Macromolecular Features Calculations

The MD simulations sample the conformations of the scFv complexes around their experimentally determined structures. Although such an analysis cannot account for large scale, long term conformational changes in the complexes, it does evaluate the features of the benchmark for computational predictions (i.e., the experimentally determined structures). The time evolution of the macromolecular features (RMSD, IE, BSA, IE/BSA, and SC) for each of the 60 trajectories are shown in Figures S1–S5, respectively, while Figure S6 shows the standard deviations of the five macromolecular features for each of the 20 complexes. To aid visualization, the IE, BSA, IE/BSA, and SC values were smoothed using a moving average of 5 values. Each point was calculated as the average of itself, the two preceding values, and the two subsequent values. Figure 3 depicts the values for the complexes with the smallest and largest average standard deviations in the features to provide an overview of the types of behaviors that were observed. Figure S7 depicts the five macromolecular features for simulation of a poorly docked complex.

All five macromolecular features show trends of relatively consistent values across the simulations. This is to be expected, as these are complexes that were experimentally discovered and have binding half-lives orders of magnitude longer than the length of the MD simulations. Although the complexes can exhibit some variation from replicate to replicate (e.g., the BSA of 7URV during the second replicate differs from the others, as shown in Figure 3) the properties remain relatively consistent overall. This contrasts with the data in Figure S7, which shows large variations in the values as the simulation progresses. The comparative consistency of the 20 scFv complexes demonstrates that they are stable throughout the MD simulations and do not exhibit gross changes in their conformations or properties. Therefore, it is appropriate to expect that interactions between amino acids can persist throughout the simulation, which would not be the case if large conformational changes were occurring or during significantly longer simulations.

3.3 | Identifying Expected Persistent and Important Interactions

Interactions are labeled according to where they were observed, the binding context of its stability, and the stability labels of the antibody and antigen residues involved. *Crystal* interactions refer to those that were observed in the energy-minimized crystal structures used as inputs to the MD simulations, while *simulation* interactions refer to those that were absent from the crystal structure and were only observed during the MD simulations. As described in the Section 2, each residue part is stable or unstable both in the context of the free protein (*pre*) and in

the antibody–antigen complex (*bound*). Finally, each pairwise interaction has two stability labels: one for the antibody residue and one for the antigen residue. The naming convention combines these three aspects (i.e., the origin where the interaction was identified, the context of its stability classification, and the combination of antibody then antigen stability) to describe the nature of an interaction. For example, a *simulation bound unstable–stable* salt bridge is an interaction observed only in MD (*simulation*) whose antibody residue has a high degree of flexibility (*unstable*) and antigen residue is conformationally constrained (*stable*) when evaluated using both proteins in the complex (*bound*).

Figure 4 shows the calculated persistences of salt bridges, hydrogen bonds, and hydrophobic interactions. The *p* values for comparing the distributions of the crystal interactions are reported in Table 1, and *p* values for comparing all interactions are in Tables S3–S5. The *p* values were calculated using one-tailed Mann–Whitney *U* tests. The data in Figure 4 do not appear to come from any single distribution, making the *U* test appropriate as it has no requirements about how data is distributed. Figure 5 depicts the energies of the crystal interactions, while the energies of the simulation interactions are shown in Figure S8. The energies are only for the snapshots from the MD trajectories in which the interactions met the corresponding geometric criteria for the interaction type. The corresponding *p* values for comparing the distributions of crystal energies are in Table 2 and the *p* values for comparing all energy distributions are in Tables S6–S8.

A number of important observations can be made from this data. The first is that simulation-only interactions are unimportant compared to crystal interactions. Figure 4 shows that they have low persistences and Tables S3–S5 demonstrate that the persistences are significantly less than those of crystal interactions. Similarly, comparing Figure 5 with Figure S8 makes it evident that the simulation-only interactions contribute much less energy during the MD simulations than the crystal interactions do. Finally, Tables S6–S8 demonstrate that the energies are significantly less beneficial than those of crystal interactions.

Analysis of the five macromolecular features showed that the complexes were stable overall during the simulations and not undergoing gross changes. This indicates that residues participating in simulation-only interactions are likely near one another in the crystal structure but do not meet the geometric criteria of the interaction. While interactions absent from crystal structures may make important contributions in other protein–protein interfaces, especially ones that undergo large conformational changes over time, for the antibody–protein complexes analyzed here such interactions do not last in the simulation and do not contribute much energy when they are present. As the simulation-only interactions were determined to be unimportant compared to the crystal one, they were not further analyzed, and all subsequent descriptions are about crystal interactions.

Prior literature, including our own, emphasized the importance of prestabilization, but that importance was not clearly observed for all interaction types in this data. Pre stable–stable salt bridges

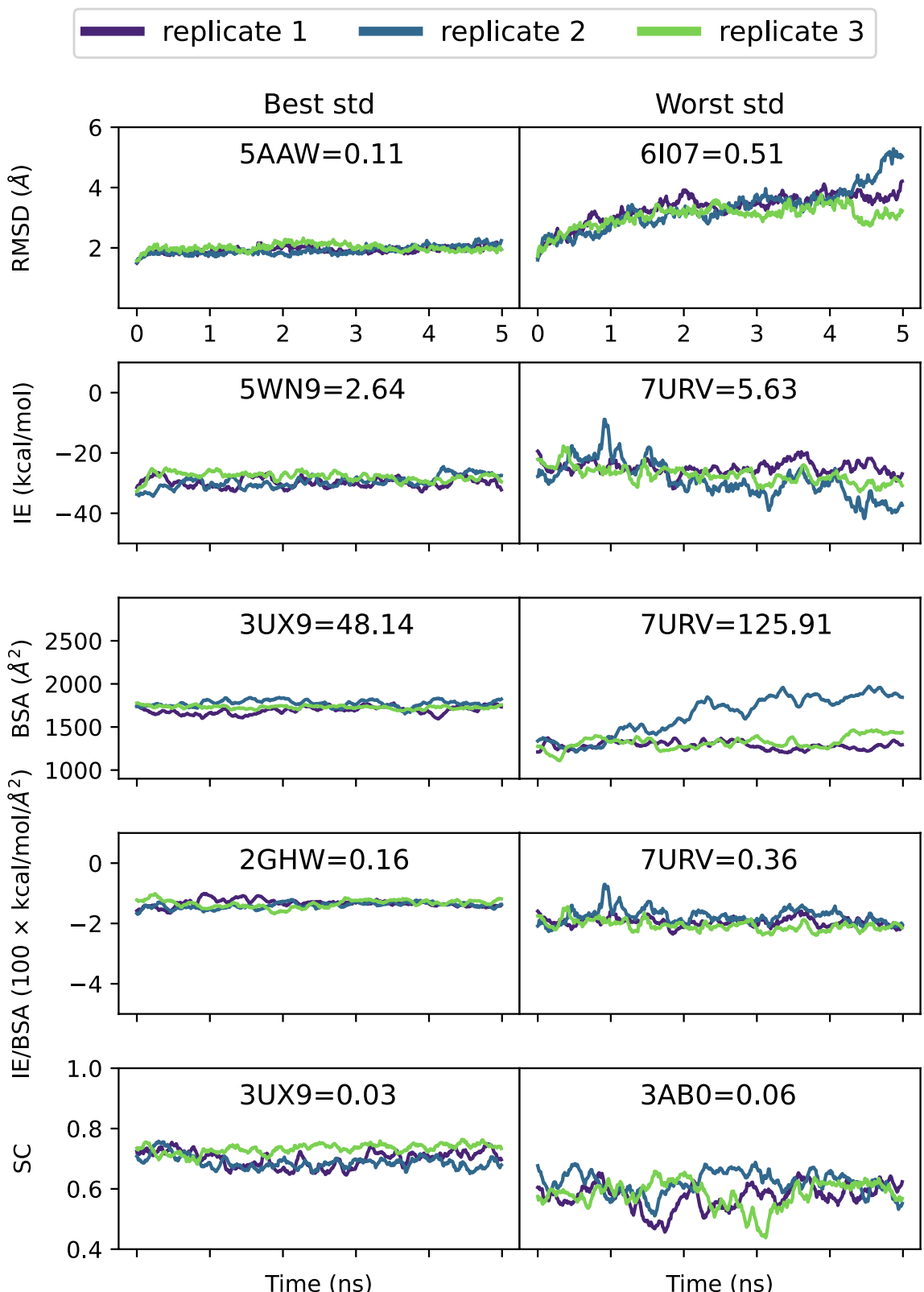


FIGURE 3 | The most and least stable complexes using the 5 macromolecular features. Each of the three trajectory replicates is depicted separately (purple: 1st, blue: 2nd, green: 3rd). The standard deviation was calculated for each trajectory and then averaged to produce the value for the complex. Overall, the macromolecular features remain relatively stable over time even though they do exhibit some variation.

do not persist significantly longer than other types of salt bridge interactions. Further, while their energies are significantly stronger than those of unstable-unstable salt bridges, they are

significantly worse than those with one unstable residue part. Pre stable-stable hydrophobic interactions do persist significantly longer than unstable-stable and unstable-unstable ones.

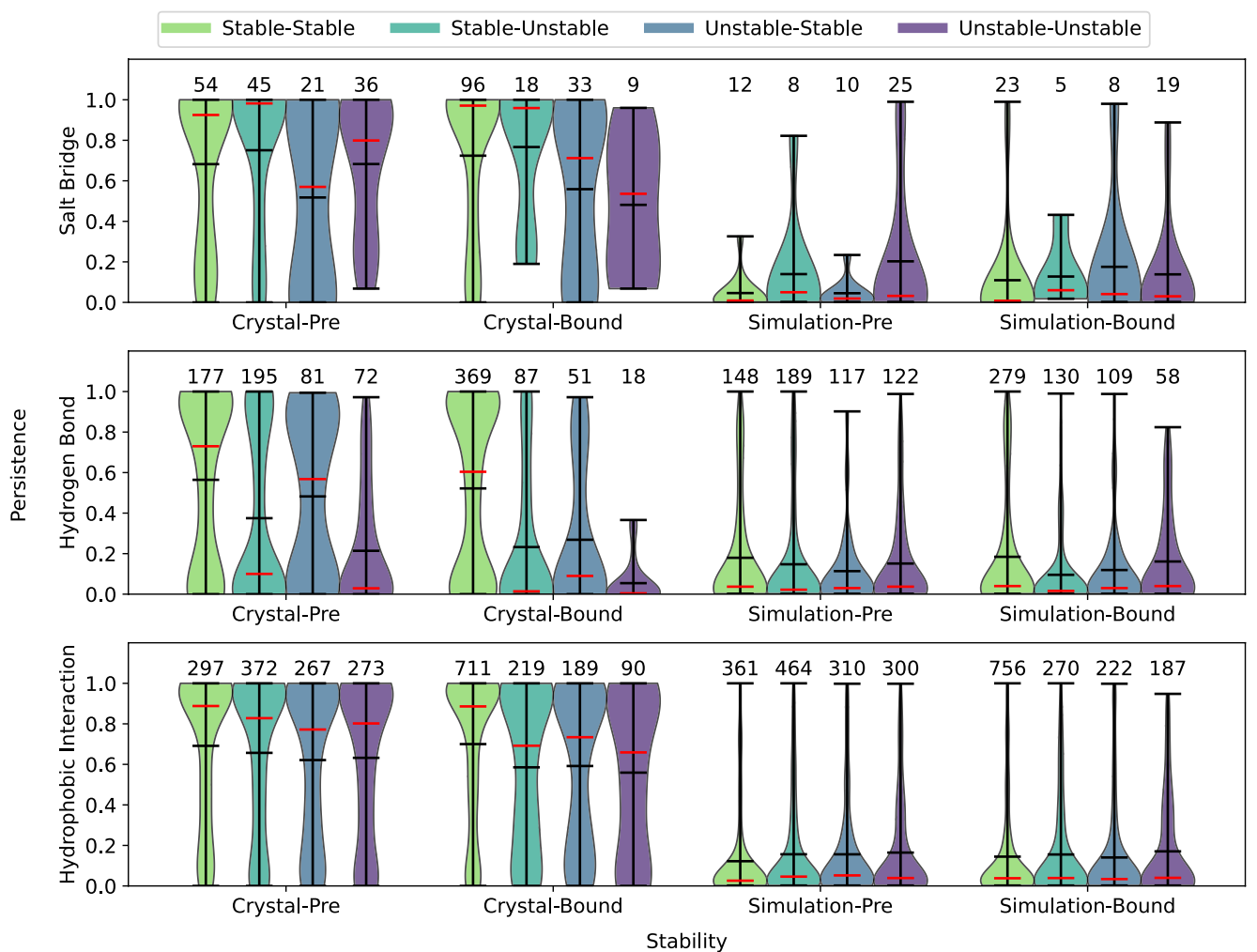


FIGURE 4 | Persistences of residue–residue interactions. The persistences of salt bridges, hydrogen bonds, and hydrophobic interactions are shown for crystal and simulation interactions based on pre- and bound stabilization criteria. Each interaction has two stable/unstable labels: The first refers to the stability of the antibody part in the interaction while the second refers to that of the antigen part. Each crystal interaction contributes three persistence values (i.e., one from each replicate) while simulation interactions are only counted for the simulations in which they are observed. Evaluation of the data shows that simulation-only interactions have lower persistences than crystal interactions. Bound-stabilization appears to be the most important criterion for determining whether or not a crystal structure hydrogen bond will persist. For crystal salt bridges and hydrophobic interactions, stabilization does not appear to determine whether or not an interaction persists but bound stable–stable interactions appear to be the most persistent for both categories. Mean values are shown with black bars and median values are shown with red bars.

However, the energies of pre unstable–unstable hydrophobic interactions are significantly stronger than those of any other classification. Overall, pre stable–stable salt bridge and hydrophobic interactions are not unambiguously better than other groups of interactions. Where prestabilization appears to be most important is for hydrogen bonds. Pre stable–stable hydrogen bonds persist significantly longer than other types of hydrogen bonds and have significantly stronger energies than the other types.

In contrast to the prior literature reports on the importance of prebinding stabilization, bound stabilization appears to be the most important criteria for persistence and strength of interactions in these complexes. There are many more bound stable–stable salt bridges than other categories, they persist significantly longer than unstable–stable and unstable–unstable ones, and they have significantly stronger energies than salt bridges with one or two unstable residue parts. Similarly, there are many more

bound stable–stable hydrophobic interactions than any other category and they persist significantly longer while demonstrating significantly stronger energies than hydrophobic interactions with one or two unstable parts.

Bound stabilization is at least as important for hydrogen bonds as prestabilization. Like pre stable–stable hydrogen bonds, those which are bound stable–stable persist significantly longer and have significantly stronger energies than other hydrogen bonds. However, while pre stable–stable hydrogen bonds did persist significantly longer than unstable–stable ones, Figure 4 illustrates that the pre unstable–stable hydrogen bonds still had relatively high persistences. That is not the case using bound stabilization criteria, where bound unstable–stable hydrogen bonds have persistences not significantly different from stable–unstable and unstable–unstable ones. This suggests that the pre unstable–stable hydrogen bonds

TABLE 1 | The p values for comparing the persistences of interactions based on their type (e.g., salt bridge), pre or bound stabilization, and which residue parts are stabilized.

		Pre						Bound			
		Stable-stable	Stable-unstable	Unstable-stable	Unstable-unstable	Stable-stable	Stable-unstable	Stable-stable	Stable-unstable	Unstable-stable	Unstable-unstable
Salt bridges	Pre	Stable–stable	—	0.84	0.06	0.23	0.83	0.65	1.86E-02	1.90E-02	
	Stable–unstable	0.16	—	0.02	3.90E-02	0.40	0.31	3.67E-03	4.89E-03		
	Unstable–stable	0.94	0.98	—	0.87	0.98	0.91	0.54	0.10	0.06E-02	
	Unstable–unstable	0.77	0.96	0.14	—	0.96	0.86	0.10	0.54	0.42	
	Bound	Stable–stable	0.17	0.60	1.62E-02	4.21E-02	—	0.36	1.65E-03	5.09E-03	
	Stable–unstable	0.36	0.70	0.10	0.15	0.64	—	3.20E-02	8.44E-03		
Hydrogen bonds	Unstable–stable	0.98	1.00	0.47	0.90	1.00	0.97	—	—	0.22	
	Unstable–unstable	0.98	1.00	0.60	0.98	1.00	0.99	0.79	—	—	
	Stable–stable	—	3.47E-04	2.95E-02	2.69E-09	0.21	1.31E-08	2.47E-06	5.17E-06		
	Stable–unstable	1.00	—	0.94	1.63E-03	1.00	1.03E-03	2.86E-02	9.54E-04		
	Unstable–stable	0.97	0.06	—	6.78E-06	0.90	1.76E-05	5.85E-04	1.77E-05		
	Unstable–unstable	1.00	1.00	1.00	—	1.00	0.44	0.72	0.07		
Hydrophobic interactions	Bound	Stable–stable	0.79	2.37E-04	0.10	1.03E-09	—	1.77E-09	3.96E-06	2.47E-06	
	Stable–unstable	1.00	1.00	1.00	0.56	1.00	—	0.75	0.11		
	Unstable–stable	1.00	0.97	1.00	0.29	1.00	0.25	—	3.49E-02		
	Unstable–unstable	1.00	1.00	1.00	0.94	1.00	0.89	0.97	—		
	Stable–stable	—	0.16	5.25E-03	2.26E-02	0.72	8.92E-04	1.48E-04	5.17E-04		
	Stable–unstable	0.84	—	0.06	0.11	0.96	8.78E-03	4.49E-03	4.05E-03		
Hydrophobic interactions	Pre	Unstable–stable	0.99	0.94	—	0.65	1.00	0.20	0.12	0.06	
	Unstable–unstable	0.98	0.89	0.35	—	1.00	0.11	0.07	3.29E-02		
	Stable–stable	0.28	4.01E-02	3.04E-04	1.54E-03	—	2.08E-05	4.32E-06	6.85E-05		
	Stable–unstable	1.00	0.99	0.80	0.89	1.00	—	0.38	0.18		
	Unstable–stable	1.00	1.00	0.88	0.93	1.00	0.62	—	0.22		
	Unstable–unstable	1.00	1.00	0.94	0.97	1.00	0.82	0.78	—		

Note: Calculations were performed using one-tailed Mann–Whitney U tests where the alternative hypothesis is that the sample in a given row persists longer than that in the corresponding column. Values with $p < 0.05$ are shown using scientific notation and the values discussed in the body of the text are bolded to make such features easier to visually identify. Bound stable–stable interactions appear to be the most persistent for all three interaction types, although prestabilized hydrogen bonds and hydrophobic interactions also have significant persistences.

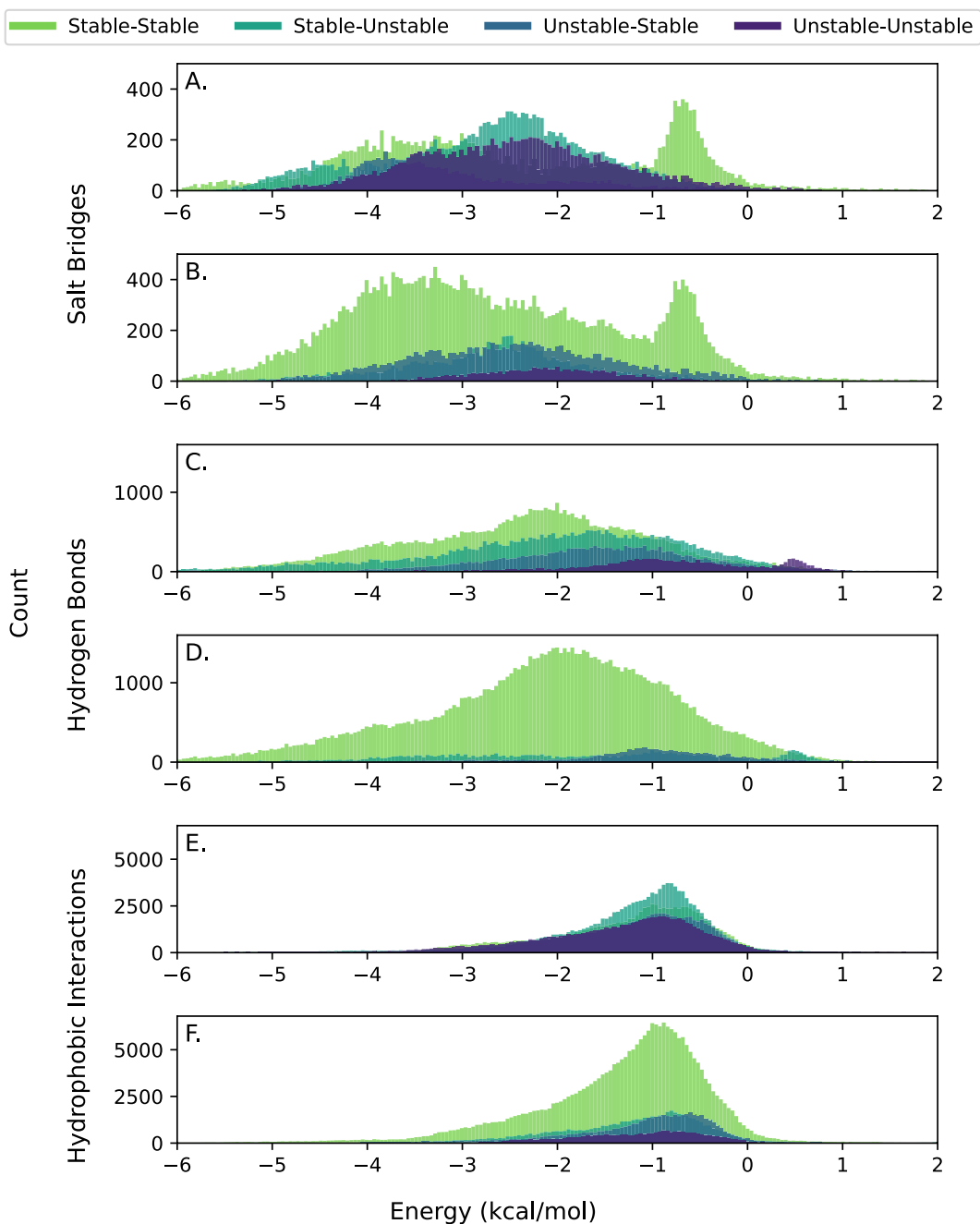


FIGURE 5 | Pairwise intermolecular MD energies for interactions that appear in the crystal structure. Panels (A, B) show salt bridge distributions for pre- and bound stability, respectively. The corresponding energies for hydrogen bonds are in panels (C, D), while those for hydrophobic interactions are in panels (E and F). The included energies are only for the MD trajectory snapshots in which the geometric criteria of the interaction were met. The prestabilization plots (A, C, and E) show meaningful energy contributions for interactions with all stability classifications. In contrast, the energies in the bound-stabilization plots (B, D, and F) are clearly dominated by stable–stable interactions. The interpretation of the data in this Figure is different from the interpretation of Table 2. The data here is the amount of energy in each distribution while Table 2 compares whether energy values are greater than one another. One notable feature of this data is that a subset of stable–stable salt bridges shows a peak between 0 and -1 kcal/mol. Manual examination of some of the interactions identified that while the charged atoms were close enough to meet the criteria, the primary energetic contributions were comparable to hydrophobic interactions because the residues lacked the flexibility to properly orient the interaction.

that persist throughout the simulation are ones that are bound stable–stable.

Although the importance of bound stabilization was not expected based on prior literature, it can be reasonably explained. Residues with limited degrees of freedom that are participating in interactions with another protein are unlikely

to move out of that interaction and thus their interactions persist. Evolution is also likely to strengthen the energies of long-lasting interactions when possible. The prior emphasis on prebinding stabilization may be because it plays a role in creating bound stable–stable interactions. Residues that are prestabilized will be bound stabilized, too. Further, they will lose fewer degrees of freedom upon binding than unstable

TABLE 2 | The p values for comparing MD energy distributions based on their type (e.g., salt bridge), pre- or bound- stabilization, and which residue parts are stabilized.

		Pre				Bound			
		Stable-stable	Stable-unstable	Unstable-stable	Unstable-unstable	Stable-stable	Stable-unstable	Stable-stable	Unstable-stable
Salt bridges									
Salt bridges	Pre	Stable–stable	—	1.00	1.00	2.65E-07	1.00	1.00	9.50E-04
	Stable–unstable	3.01E-37	—	1.00	1.00	3.88E-80	0.95	1.78E-05	1.60E-54
	Unstable–stable	2.10E-159	6.93E-160	—	—	0.00E+00	2.19E-107	2.44E-207	9.92E-304
	Unstable–unstable	1.00	1.00	1.00	—	—	1.00	1.00	0.95
	Bound	Stable–stable	1.43E-45	4.64E-02	1.00	2.82E-105	—	4.10E-16	3.70E-69
	Stable–unstable	1.09E-03	1.00	1.00	1.76E-29	1.00	—	5.01E-19	2.48E-111
Hydrogen bonds									
Hydrogen bonds	Pre	Unstable–stable	1.00	1.00	1.00	4.77E-02	1.00	1.00	—
	Stable–stable	—	7.48E-231	0.00E+00	0.00E+00	6.27E-200	1.48E-287	0.00E+00	1.01E-231
	Stable–unstable	1.00	—	6.14E-238	0.00E+00	1.00	5.25E-84	0.00E+00	1.07E-195
	Unstable–stable	1.00	1.00	—	0.00E+00	1.00	1.00	0.00E+00	4.69E-159
	Unstable–unstable	1.00	1.00	1.00	—	1.00	1.00	1.00	1.27E-58
	Bound	Stable–stable	1.00	6.35E-27	0.00E+00	0.00E+00	—	2.72E-142	0.00E+00
Hydrophobic interactions									
Hydrophobic interactions	Pre	Stable–unstable	1.00	1.00	5.95E-05	0.00E+00	1.00	—	2.41E-193
	Stable–stable	1.00	1.00	1.00	1.08E-79	1.00	1.00	—	6.95E-145
	Unstable–unstable	1.00	1.00	1.00	1.00	1.00	1.00	1.00	—
	Stable–stable	—	1.42E-07	8.79E-19	1.00	1.00	2.10E-17	4.23E-223	2.23E-89
	Stable–unstable	1.00	—	1.60E-04	1.00	1.00	1.63E-04	1.82E-207	2.26E-29
	Unstable–stable	1.00	1.00	—	1.00	1.00	0.43	1.45E-130	2.04E-07
Bound	Pre	Unstable–unstable	3.15E-118	3.35E-203	8.07E-207	—	6.78E-28	3.09E-179	0.00E+00
	Stable–stable	7.35E-78	2.73E-164	5.24E-167	1.00	—	2.31E-136	0.00E+00	4.73E-149
	Stable–unstable	1.00	1.00	0.57	1.00	1.00	—	2.48E-106	9.62E-07
	Unstable–stable	1.00	1.00	1.00	1.00	1.00	1.00	—	1.00
	Unstable–unstable	1.00	1.00	1.00	1.00	1.00	1.00	2.22E-37	—
	Bound	Stable–stable	—	—	—	—	—	—	—

Note: Calculations were performed using one-tailed Mann–Whitney U tests where the alternative hypothesis is that the sample in a given row is more energetically favorable than that in the corresponding column. Values with $p < 0.05$ are shown using scientific notation and the values discussed in the body of the text are bolded to make such features easier to visually identify. Bound stable–stable interactions appear to be the most favorable for all three interaction types.

residues and have a correspondingly lower entropic cost for binding.

From the perspective of designing binding proteins, the residue–residue interaction persistence and energy data indicate that protein binding interfaces should have many bound stable–stable interactions because they are the longest-lasting and strongest interactions. However, while bound stable–stable salt bridges and hydrophobic interactions persist longer than others, the data in Figure 4 makes it clear that salt bridges and hydrophobic interactions with unstable residue parts can still be long-lasting and persistent throughout the simulations. Therefore, expected persistent interactions were defined as: all salt bridges, bound stable–stable hydrogen bonds, and all hydrophobic interactions, where all interactions must be present in the energy-minimized crystal structure.

3.4 | Features of Expected Persistent Interactions

To determine whether the expected persistent interactions contribute consistently to the antibody–protein complex, their energies were summed in each of the 500 structures from each MD simulation, which are depicted in Figure 6. In each structure, only the energies of the expected persistent interactions that met their corresponding geometric criteria in that snapshot were included. Separate sums for each interaction type (i.e., salt bridges, hydrogen bonds, and hydrophobic interactions) were calculated and this was repeated for each of the three replicates for each complex. To make the plots directly comparable to the IE plots in Figure 3 and Figure S2, the plots were smoothed using a moving average of five values. The results are comparable to those of the five macromolecular features of RMSD, IE, BSA, IE/BSA, and SC: there is some variation over time and from replicate to replicate, but the general trend is that the lines are flat and staying in a relatively narrow range of values. In particular, the energies of the expected persistent interactions do not appear to behave qualitatively differently than the IE of the complexes as a whole.

An important consideration is how the energies of the expected persistent interactions in the MD simulations compare to their values in the energy-minimized crystal structure. The average energy during the MD simulations was calculated for all interactions with a crystal structure energy greater in magnitude than 0.1 kcal/mol, and the ratio of the average MD energy to the minimized crystal energy was plotted in Figure 7. Interactions with a crystal energy smaller in magnitude than 0.1 were excluded because relatively small changes in their MD energy led to large changes in the calculated ratios and caused outlier effects. Figure 7 has separate results for bound stable–stable, stable–unstable, unstable–stable, and unstable–unstable salt bridges, hydrogen bonds, and hydrophobic interactions. The figure includes both histograms and a kernel density estimated distribution using SciPy (gaussian_kde) for each category, and the peaks of the estimated distributions are marked.

For hydrogen bonds, the estimated distribution of the expected persistent interactions (i.e., bound stable–stable) appears to follow a normal distribution and peaks at a higher percentage than those of other hydrogen bonds. The expected persistent binding energy (EPBE) of expected persistent hydrogen bonds was

defined as 73.9% (i.e., the peak of the estimated distribution in Figure 7) of their crystal structure energy. The estimated distributions for all types of hydrophobic interactions appear normal and have maximum values close to one another, although the unstable–unstable distribution does appear to have the widest spread of values. Because the peaks are close to one another and all distributions appear normal, the EPBE of hydrophobic interactions was defined as the peak of the estimated distribution for all hydrophobic interactions: 86.6% of their crystal energy (data not shown). Finally, while salt bridges with zero or one bound unstable parts are estimated to follow approximately normal distributions with similar peaks, bound unstable–unstable salt bridges do not appear to follow a normal distribution. Those interactions have a noticeably lower ratio of average MD to crystal structure energies than other salt bridges. However, bound unstable–unstable salt bridges are rare in the 20 studied complexes, with only three such interactions observed. Therefore, the EPBE of salt bridges was defined as the peak of the estimated distribution of all salt bridges: 75.4% of their crystal energy (data not shown).

A key finding of this work is that bound stable–stable interactions persist longer and have stronger energies than other interactions. Further, there is evidence of asymmetric stabilization in the persistence data in Figure 4 (e.g., a comparison of the persistence rates of the pre and bound unstable–stable hydrogen bonds compared to stable–unstable ones). Therefore, an evaluation of the statistical significance of the stabilization of interacting residues in antibodies compared to antigens was conducted.

Briefly, 19/38 (50.0%) of bound stable antibody residue parts participating in expected persistent salt bridges (i.e., any salt bridge) were stabilized by binding (i.e., went from pre unstable to bound stable) compared to 27/43 (62.8%) for antigen residues. The denominators of these fractions are different because there are more bound unstable (antibody)—stable (antigen) salt bridges than stable (antibody)—unstable (antigen) ones. The comparable numbers for other expected persistent interactions were 22/123 (17.9%) for antibody residues and 46/123 (37.4%) for antigen residues in hydrogen bonds and 180/310 (58.1%) for antibody residues versus 215/300 (71.7%) for antigen residues in hydrophobic interactions. In all cases, antigen residues participating in expected persistent interactions were stabilized at a higher rate than antibody residues. Notably, antigen salt bridge and hydrophobic interaction residues were stabilized 12.8% and 13.6% more frequently than antibody residues, values that are much more similar to one another than the 19.5% increase for hydrogen bonds.

For each interaction type, statistical tests were performed to assess (1) whether antibody residues are stabilized less frequently than antigen residues and (2) whether antigen residues are stabilized more frequently than antibody residues. For salt bridges, neither test was statistically significant ($p = 0.0733$ and 0.0631 , respectively). In contrast, both tests were statistically significant for hydrogen bonds ($p = 2.02\text{e-}6$ and $2.49\text{e-}7$, respectively) and hydrophobic interactions ($p = 2.05\text{e-}7$ and $7.29\text{e-}7$, respectively). Given the relatively small number of salt bridges compared to both hydrogen bonds and hydrophobic interactions, preferential stabilization of antigen salt bridge

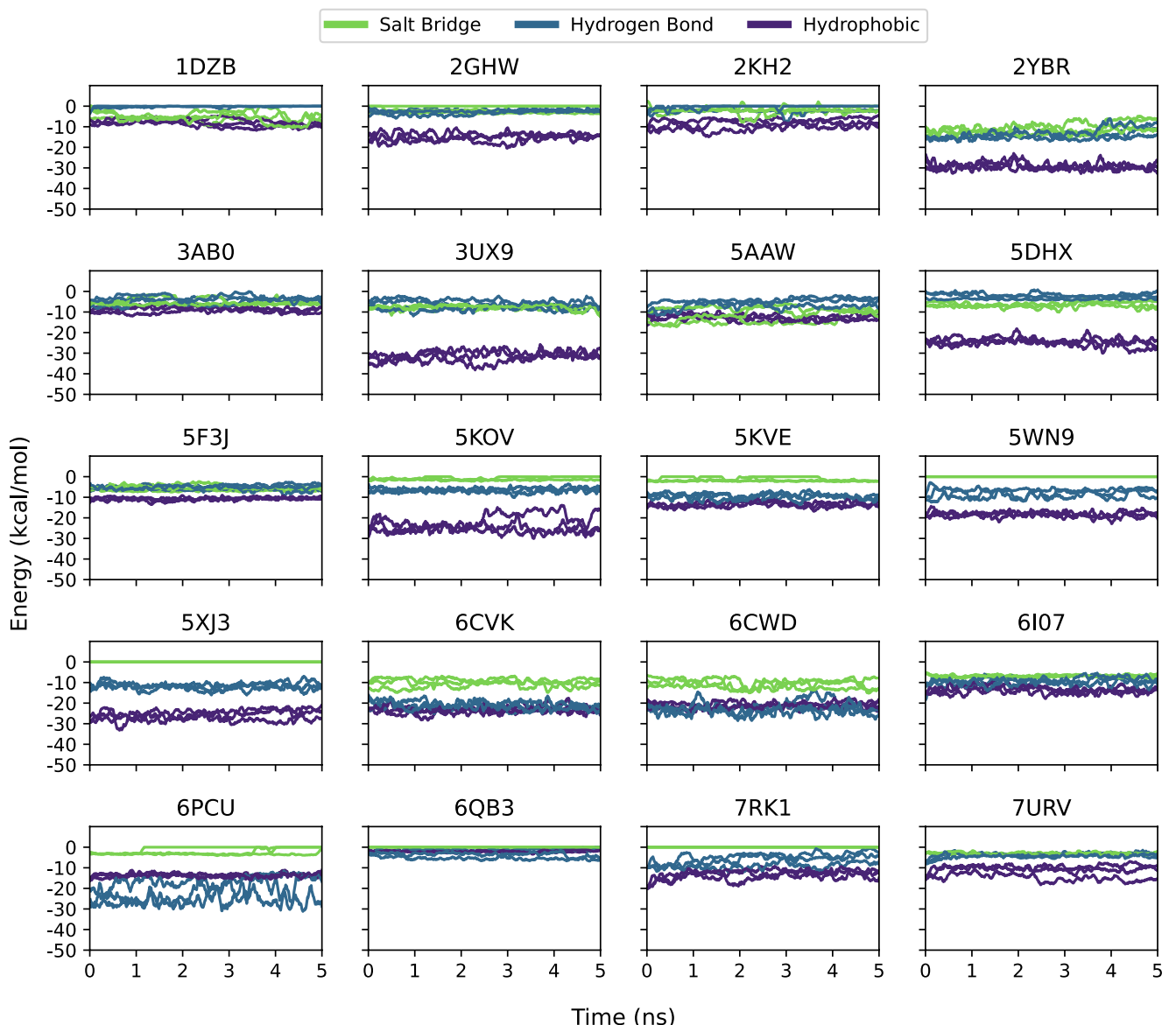


FIGURE 6 | Energies of expected persistent interactions. The energies of the interactions that were expected to persist were summed in each structure of the simulation trajectories for each interaction type (i.e., salt bridges, hydrogen bonds, and hydrophobic interactions). The results are smoothed using a five-point moving average to make these energies directly comparable to those in Figure 2. The energies all appear to be consistent over the course of the simulations and most importantly they do not appear to be qualitatively different from the IEs in Figures 2 and S2. This indicates that the expected persistent interactions are collectively contributing a relatively constant amount of energy both overall and by interaction type.

residues may still occur, but it was not statistically significant in this data. The concept that antigen residues would be stabilized more frequently than antibody residues is consistent with the observation that evolution can prestabilize antibody residues during affinity maturation but does not have the same effect on antigen residues.

3.5 | Using Interaction Features to Eliminate False Positive Complexes

The HADDOCK and RosettaDock protocols each predicted 200 configurations for each antibody–antigen complex, while ClusPro predicted between 49 and 120 configuration for each complex. Briefly, 9953 total docked complexes were predicted,

of which 8194 were poorly docked because they positioned the antigen near the antibody CDRs while having an antigen RMSD $> 10 \text{ \AA}$. A total of 265 complexes were acceptably docked (i.e., antigen RMSD $\leq 10 \text{ \AA}$) and 1490 were discarded for having infeasible binding modes.

Many features based on the properties of the expected persistent pairwise interactions defined in this work were calculated for the 220 naturally occurring, 8194 poorly docked, and 265 acceptably docked complexes, the full list of which is in Table S9. They include the number of expected persistent salt bridges, hydrogen bonds, and hydrophobic interactions, as well as the total combined number of expected persistent interactions. It was observed that many of the naturally occurring antibody complexes had no salt bridges and it was hypothesized that they may compensate for

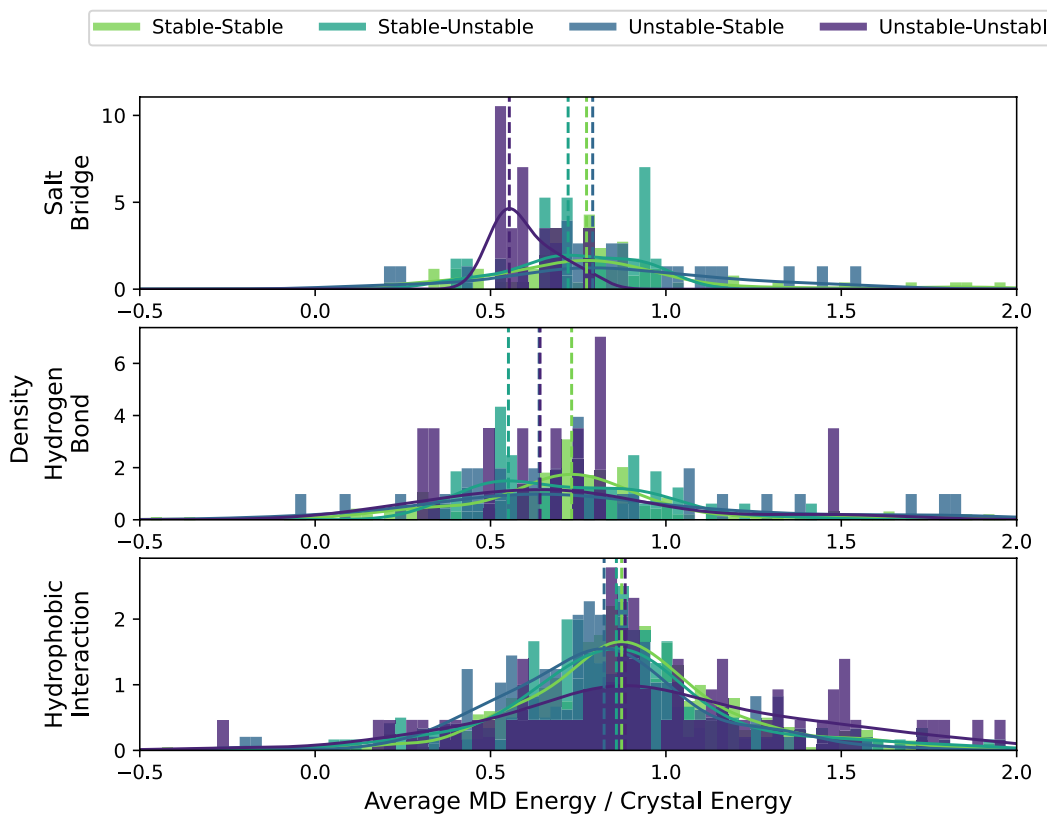


FIGURE 7 | Average fraction of crystal structure energy contributed by interactions during MD simulations. The average MD energy of each energy was divided by its crystal structure energy. Interactions with crystal energy smaller in magnitude than 0.1 kcal/mol were removed as outliers. Interactions are classified based on their bound stabilities. Both histograms and kernel density estimated distributions are shown. The only distribution that does not appear to be normal is that of unstable-unstable salt bridges, which skews significantly lower than other salt bridges.

this by having more hydrogen bonds. Therefore, the number of expected persistent polar interactions (i.e., salt bridges plus hydrogen bonds) was included. The EPBE of each of these categories was also used as a feature. Further, the number of rotamers lost by binding, used as a proxy for the stabilization caused by binding, was calculated for each interaction type separately in antibodies and antigens, as well as combined. Additionally, interface features that are not expected to contribute to persistent interactions (i.e., hydrogen bonds with unstable residues and non-interacting residues) were calculated. Finally, normalized versions of all of these metrics were calculated by dividing by BSA based on the observation that complexes with more BSA would be expected to have more of everything than complexes with smaller BSA. In addition to the features of expected persistent pairwise interactions, the macromolecular features of IE, BSA, IE/BSA, and SC were calculated for each complex.

Three random forest classifiers were trained using the 8194 poorly docked and 220 naturally occurring complexes: one using only the four macromolecular features, one using only the expected persistent pairwise interaction features, and one using both the macromolecular features and the expected persistent pairwise interaction features (i.e., all features). Table 3 lists the average false positive rates of the random forest classifiers at varying levels of true positive classification rates. Figure S9 shows average receiver operating characteristic (ROC) curves

for the classifier using macromolecular features compared to the classifier using all features.

The classifier trained with all features has a lower false positive rate than those using only macromolecular features or expected persistent interaction features at every true positive rate. The best discrimination over the classifier with macromolecular features occurs at a true positive rate of 40%, where inclusion of the interaction features results in a 5.6-fold reduction in false positive rate, but the features provide at least a 2.0-fold improvement at all true positive rates. We consider it especially promising that the classifier considers only 10% of false complexes to have features comparable to 90% of naturally occurring antibodies when the expected persistent pairwise interaction features are included compared to 29% of false complexes without them.

The classifier trained solely on the expected persistent interaction features had higher false positive rates than the classifier trained using only the macromolecular features at most true positive rates. However, this trend reversed for high true positive rates. In other words, the classifier trained using the expected persistent interaction features was better at eliminating false complexes than the one trained using the macromolecular features when nearly all true complexes were correctly classified.

TABLE 3 | False positive rates from the three random forest classifiers.

True positive rate	Macromolecular features false positive rate	Expected persistent pairwise interaction features false positive rate	All features false positive rate	Fold improvement of all features over macromolecular features
0.250	2.90E-04	4.60E-04	1.26E-04	2.29
0.300	5.26E-04	8.65E-04	1.55E-04	3.40
0.350	7.60E-04	1.67E-03	1.65E-04	4.58
0.400	1.15E-03	2.51E-03	2.06E-04	5.60
0.450	1.49E-03	3.84E-03	3.10E-04	4.81
0.500	2.18E-03	5.79E-03	5.87E-04	3.72
0.550	3.24E-03	8.30E-03	1.12E-03	2.88
0.600	6.11E-03	0.013	2.25E-03	2.71
0.650	0.011	0.022	4.16E-03	2.53
0.700	0.017	0.035	8.25E-03	2.10
0.750	0.032	0.051	0.015	2.11
0.800	0.065	0.079	0.029	2.29
0.850	0.120	0.130	0.047	2.54
0.900	0.289	0.238	0.103	2.81
0.950	0.645	0.468	0.317	2.04

Note: False positive rates were determined from the average receiver operating characteristic curve of the 50 classifiers for varying true positive rates. At every point, the classifier using all features outperformed the ones using only the macromolecular features or only the expected persistent interaction features. At a 90% true positive rate, only 10% of false complexes were misclassified using all features compared to 29% with only the macromolecular features and 24% with only the expected persistent interaction features.

LOOCV was performed to further evaluate the usefulness of including pairwise residue interaction features. The LOOCV analysis using only the macromolecular features correctly classified 118/220 (53.6%) real antibodies as binders and misclassified 25/8194 (0.305%) poorly docked complexes as binders. A comparable analysis using only the expected persistent interaction features correctly classified only 76/220 (34.5%) of real antibodies as binders but also only misclassified 12/8194 (0.146%) of poorly docked complexes as likely binders. Conducting the LOOCV analysis with both the macromolecular and expected persistent interaction features improved those numbers to 121/220 (55.0%) and 10/8194 (0.122%). Compared to the analysis using only the macromolecular features, the improvement in correctly classifying real complexes was not statistically significant ($p=0.319$) but the reduction in false positives was significant ($p=5.78e-4$). 25 and 10 false positives are in line with the average performance of the random forest classifier at a true positive rate of 55%, as shown in Table 3, as the reported percentages correspond to average false positive numbers of 26.6 and 9.2. Overall, the random forest classifiers and LOOCV analyses reveal similar findings: that the best discrimination between real and decoy complexes is achieved using both the macromolecular and expected persistent interaction features and that the benefits of the expected persistent features are complementary to, rather than duplicative of, those of the macromolecular features.

To further evaluate the utility of the expected persistent pairwise interaction features, a classifier was trained using all features on all 8194 poorly docked and 220 naturally occurring complexes and used to classify the 265 acceptably docked complexes. The acceptably docked complexes were subcategorized as those having antigen RMSDs $\leq 3\text{ \AA}$ (77 complexes), $\leq 5\text{ \AA}$ (32 complexes), and $\leq 10\text{ \AA}$ (156 complexes). These RMSD cutoffs come from the CAPRI evaluation method [78] with the caveat that very few docked structures had antigen RMSD $\leq 1\text{ \AA}$, so the lowest cutoff was increased to 3 \AA . Using the default hyperparameters and thresholds, the percentages of the subcategories that are classified as likely binders are 51.9%, 9.4%, and 2.6%, respectively. These values are most comparable to the 55.0% true positive and 0.122% false positive rates from the LOOCV analysis. This demonstrates that as antigens become closer to their experimentally determined conformations that they are more likely to be classified as likely binders.

Table S9 lists the average Gini importance of the features used to train the classifier. IE, BSA, IE/BSA, and SC were the 2nd, 11th, 1st, and 5th most important features. Also in the top 11 features were total EPBE (3rd), total EPBE/BSA (7th), EPBE of hydrogen bonds (4th), number of hydrogen bonds (6th), EPBE of hydrogen bonds/BSA (8th), number of hydrogen bonds/BSA (10th), and EPBE of hydrophobic interactions (9th). Notably, the total EPBE and properties of hydrogen bonds were features that

the classifier could use to distinguish real antibody complexes from poorly docked ones. This is further evidence that the properties of the expected persistent interactions overall and those of hydrogen bonds specifically, which had the strictest criteria, provide useful information for discriminating false complexes from real ones.

This work has demonstrated that properties of pairwise interactions in antibody–protein interfaces can help with correctly classifying decoy complexes. However, the classifications used here are still relatively underdeveloped. The interaction definitions are binary, resulting in different classifications for amino acids with nearly identical geometries (e.g., hydrogen bond donor–acceptor pairs that are 2.49 and 2.51 Å apart have different classifications) and no discrimination between exceptionally good interactions versus those that barely meet the criteria. Similarly, the evaluation of steric clashes with rotamers does not account for the flexibility of neighboring residues. Analysis of the data in Figure 4 makes it evident that the classifications are imperfect. For example, a significant fraction of bound stable–stable hydrogen bonds (i.e., expected persistent ones) was observed to have short persistences.

It is likely that transitioning the classification criteria to continuous metrics rather than binary choices and accounting for the stability of neighboring residues would result in improved features. Additionally, no feature engineering or hyperparameter optimization for the random forest classifier was performed, which would also be expected to improve the results. Nonetheless, even with the limited definitions used in this work, meaningful benefits were observed in the ability to avoid classifying false computational predictions as likely experimental binders. Expanding the analysis here to general protein–protein complexes, refining the interaction definitions, optimizing the classifications, and implementing the methods into distributable tools (e.g., docking software) are expected to be the focus of future works now that it has been demonstrated that the features of how amino acids interact in antibody–protein interfaces can provide useful insights.

4 | Conclusions

Although ML-based protein design programs are rapidly improving, they continue to face the challenge of predicting many false complexes, much as docking programs have for many years. For protein structure prediction, it has been demonstrated that residue–residue contact information can be a critical component of accurate ML methods. We hypothesized that features of salt bridges, hydrogen bonds, and hydrophobic interactions in antibody–protein complexes could help distinguish them from false complexes. Twenty antibody–protein complexes were analyzed with MD simulations to identify important pairwise interaction features. It was shown that all salt bridges, hydrogen bonds with both residues stabilized in the bound complex, and all hydrophobic interactions are expected to be persistent. More generally, bound stable–stable interactions are both more persistent and have stronger energies than other interactions. The data also demonstrated that antigen residues are stabilized by binding more frequently than antibody residues. Including features of the expected persistent interactions led to an at least

two-fold reduction in false complexes misclassified as likely binders by a random forest classifier compared to only using the macromolecular features of IE, BSA, IE/BSA and SC. An example of the improvement is that when accounting for pairwise interaction features, the classifier mistakenly identified only 10% of false complexes as having features similar to 90% of real antibody–protein complexes. This compares to misclassifying 29% of false complexes when those features are not considered. It is expected that the features identified here will be of use in future analyses of protein–protein interactions and the design of binding proteins.

Author Contributions

A. Clay Richard: conceptualization, investigation, writing – original draft, methodology, validation, visualization, writing – review and editing, software, formal analysis, data curation. **Robert J. Pantazes:** conceptualization, investigation, funding acquisition, writing – review and editing, methodology, validation, visualization, formal analysis, project administration, supervision, resources, writing – original draft.

Acknowledgments

This work was funded by the NSF EPSCoR RII Track-2 Award 2119237. It was completed in part with resources on the Auburn University Easley Cluster. NAMD was developed by the Theoretical and Computational Biophysics Group in the Beckman Institute for Advanced Science and Technology at the University of Illinois at Urbana-Champaign.

Conflicts of Interest

The authors declare no conflicts of interest.

Data Availability Statement

The data that support the findings of this study are available from the corresponding author upon reasonable request.

Peer Review

The peer review history for this article is available at <https://www.webofscience.com/api/gateway/wos/peer-review/10.1002/prot.26773>.

References

1. J. Dauparas, I. Anishchenko, N. Bennett, et al., “Robust Deep Learning-Based Protein Sequence Design Using ProteinMPNN,” *Science* 378, no. 6615 (2022): 49–56, <https://doi.org/10.1126/science.add2187>.
2. S. Wang, S. Sun, Z. Li, R. Zhang, and J. Xu, “Accurate De Novo Prediction of Protein Contact Map by Ultra-Deep Learning Model,” *PLoS Computational Biology* 13, no. 1 (2017): e1005324, <https://doi.org/10.1371/journal.pcbi.1005324>.
3. J.-E. Shin, A. J. Riesselman, A. W. Kollasch, et al., “Protein Design and Variant Prediction Using Autoregressive Generative Models,” *Nature Communications* 12 (2021): 2403, <https://doi.org/10.1038/s41467-021-22732-w>.
4. J. R. Rogers, G. Nikolényi, and M. AlQuraishi, “Growing Ecosystem of Deep Learning Methods for Modeling Protein–Protein Interactions,” *Protein Engineering, Design & Selection* 36 (2023): gzad023, <https://doi.org/10.1093/protein/gzad023>.
5. J. L. Watson, D. Juergens, N. R. Bennett, et al., “Novo Design of Protein Structure and Function With RFdiffusion,” *Nature* 620, no. 7976 (2023): 1089–1100, <https://doi.org/10.1038/s41586-023-06415-8>.

6. S. Luo, Y. Su, X. Peng, S. Wang, J. Peng, and J. Ma, "Antigen-Specific Antibody Design and Optimization With Diffusion-Based Generative Models for Protein Structures," in *Advances in Neural Information Processing Systems*, vol. 35, eds. S. Koyejo, S. Mohamed, A. Agarwal, D. Belgrave, K. Cho, and A. Oh (New York, USA: Curran Associates, Inc., 2022), 9754–9767.
7. J. Jumper, R. Evans, A. Pritzel, et al., "Highly Accurate Protein Structure Prediction With AlphaFold," *Nature* 596, no. 7873 (2021): 583–589, <https://doi.org/10.1038/s41586-021-03819-2>.
8. M. Baek, F. DiMaio, I. Anishchenko, et al., "Accurate Prediction of Protein Structures and Interactions Using a Three-Track Neural Network," *Science* 373, no. 6557 (2021): 871–876, <https://doi.org/10.1126/science.abj8754>.
9. N. S. Pagadala, K. Syed, and J. Tuszyński, "Software for Molecular Docking: A Review," *Biophysical Reviews* 9, no. 2 (2017): 91–102, <https://doi.org/10.1007/s12551-016-0247-1>.
10. B. D. Bursulaya, M. Totrov, R. Abagyan, and C. L. Brooks III, "Comparative Study of Several Algorithms for Flexible Ligand Docking," *Journal of Computer-Aided Molecular Design* 17, no. 11 (2003): 755–763, <https://doi.org/10.1023/B:JCAM.0000017496.76572.6f>.
11. M. E. Buckley, A. R. N. Ndukwé, P. C. Nair, S. Rana, K. E. Fairfull-Smith, and N. S. Gandhi, "Comparative Assessment of Docking Programs for Docking and Virtual Screening of Ribosomal Oxazolidinone Antibacterial Agents," *Antibiotics* 12, no. 3 (2023): 463, <https://doi.org/10.3390/antibiotics12030463>.
12. M. F. Lensink, S. Velankar, and S. J. Wodak, "Modeling Protein-Protein and Protein-Peptide Complexes: CAPRI 6th Edition," *Proteins: Structure, Function, and Bioinformatics* 85, no. 3 (2017): 359–377, <https://doi.org/10.1002/prot.25215>.
13. M. F. Lensink, S. Velankar, M. Baek, L. Heo, C. Seok, and S. J. Wodak, "The Challenge of Modeling Protein Assemblies: The CASP12-CAPRI Experiment," *Proteins: Structure, Function, and Bioinformatics* 86, no. S1 (2018): 257–273, <https://doi.org/10.1002/prot.25419>.
14. M. F. Lensink, N. Nadzirin, S. Velankar, and S. J. Wodak, "Modeling Protein-Protein, Protein-Peptide, and Protein-Oligosaccharide Complexes: CAPRI 7th Edition," *Proteins: Structure, Function, and Bioinformatics* 88, no. 8 (2020): 916–938, <https://doi.org/10.1002/prot.25870>.
15. M. F. Lensink, G. Brysbaert, T. Mauri, et al., "Prediction of Protein Assemblies, the Next Frontier: The CASP14-CAPRI Experiment," *Proteins: Structure, Function, and Bioinformatics* 89, no. 12 (2021): 1800–1823, <https://doi.org/10.1002/prot.26222>.
16. Z. Lin, H. Akin, R. Rao, et al., "Evolutionary-Scale Prediction of Atomic-Level Protein Structure With a Language Model," *Science* 379, no. 6637 (2023): 1123–1130, <https://doi.org/10.1126/science.adc2574>.
17. G. J. Bartlett, C. T. Porter, N. Borkakoti, and J. M. Thornton, "Analysis of Catalytic Residues in Enzyme Active Sites," *Journal of Molecular Biology* 324, no. 1 (2002): 105–121, [https://doi.org/10.1016/s0022-2836\(02\)01036-7](https://doi.org/10.1016/s0022-2836(02)01036-7).
18. M. L. Fernández-Quintero, J. R. Loeffler, L. M. Bacher, F. Waibel, C. A. Seidler, and K. R. Liedl, "Local and Global Rigidification Upon Antibody Affinity Maturation," *Frontiers in Molecular Biosciences* 7 (2020): 182.
19. A. K. Mishra and R. A. Mariuzza, "Insights Into the Structural Basis of Antibody Affinity Maturation From Next-Generation Sequencing," *Frontiers in Immunology* 9 (2018): 117, <https://doi.org/10.3389/fimmu.2018.00117>.
20. X. Qiao, L. Qu, Y. Guo, and T. Hoshino, "Secondary Structure and Conformational Stability of the Antigen Residues Making Contact With Antibodies," *Journal of Physical Chemistry. B* 125, no. 41 (2021): 11374–11385, <https://doi.org/10.1021/acs.jpcb.1c05997>.
21. V. N. Uversky and M. H. V. Van Regenmortel, "Mobility and Disorder in Antibody and Antigen Binding Sites Do Not Prevent Immunochemical Recognition," *Critical Reviews in Biochemistry and Molecular Biology* 56, no. 2 (2021): 149–156, <https://doi.org/10.1080/10409238.2020.1869683>.
22. M. Wang, D. Zhu, J. Zhu, R. Nussinov, and B. Ma, "Local and Global Anatomy of Antibody-Protein Antigen Recognition," *Journal of Molecular Recognition* 31, no. 5 (2018): e2693, <https://doi.org/10.1002/jmr.2693>.
23. S. J. Fleishman, S. D. Khare, N. Koga, and D. Baker, "Restricted Side-chain Plasticity in the Structures of Native Proteins and Complexes," *Protein Science* 20, no. 4 (2011): 753–757, <https://doi.org/10.1002/pro.604>.
24. S. J. Fleishman, J. E. Corn, E.-M. Strauch, T. A. Whitehead, J. Karanicolas, and D. Baker, "Hotspot-Centric De Novo Design of Protein Binders," *Journal of Molecular Biology* 413, no. 5 (2011): 1047–1062, <https://doi.org/10.1016/j.jmb.2011.09.001>.
25. X. Liu, R. D. Taylor, L. Griffin, et al., "Computational Design of an Epitope-Specific Keap1 Binding Antibody Using Hotspot Residues Grafting and CDR Loop Swapping," *Scientific Reports* 7 (2017): 41306, <https://doi.org/10.1038/srep41306>.
26. R. J. Pantazes, M. C. Saraf, and C. D. Maranas, "Optimal Protein Library Design Using Recombination or Point Mutations Based on Sequence-Based Scoring Functions," *Protein Engineering, Design & Selection* 20, no. 8 (2007): 361–373, <https://doi.org/10.1093/protein/gzm030>.
27. S. Islam and R. J. Pantazes, "Developing Similarity Matrices for Antibody-Protein Binding Interactions," *PLoS One* 18, no. 10 (2023): e0293606, <https://doi.org/10.1371/journal.pone.0293606>.
28. V. M. Chauhan and R. J. Pantazes, "Analysis of Conformational Stability of Interacting Residues in Protein Binding Interfaces," *Protein Engineering, Design & Selection* 36 (2023): gzad016, <https://doi.org/10.1093/protein/gzad016>.
29. I. A. Wilson and R. L. Stanfield, "Antibody-Antigen Interactions," *Current Opinion in Structural Biology* 3, no. 1 (1993): 113–118, [https://doi.org/10.1016/0959-440X\(93\)90210-C](https://doi.org/10.1016/0959-440X(93)90210-C).
30. R. J. Pantazes and C. D. Maranas, "OptCDR: A General Computational Method for the Design of Antibody Complementarity Determining Regions for Targeted Epitope Binding," *Protein Engineering, Design & Selection* 23, no. 11 (2010): 849–858, <https://doi.org/10.1093/protein/gzq061>.
31. K. C. Entzminger, J. Hyun, R. J. Pantazes, et al., "Novo Design of Antibody Complementarity Determining Regions Binding a FLAG Tetra-Peptide," *Scientific Reports* 7, no. 1 (2017): 10295, <https://doi.org/10.1038/s41598-017-10737-9>.
32. T. Li, R. J. Pantazes, and C. D. Maranas, "OptMAVEN—A New Framework for the De Novo Design of Antibody Variable Region Models Targeting Specific Antigen Epitopes," *PLoS One* 9, no. 8 (2014): e105954, <https://doi.org/10.1371/journal.pone.0105954>.
33. V. G. Poosarla, T. Li, B. C. Goh, K. Schulten, T. K. Wood, and C. D. Maranas, "Computational De Novo Design of Antibodies Binding to a Peptide With High Affinity," *Biotechnology and Bioengineering* 114, no. 6 (2017): 1331–1342, <https://doi.org/10.1002/bit.26244>.
34. J. Adolf-Bryfogle, O. Kalyuzhnii, M. Kubitz, et al., "RosettaAntibodyDesign (RAbD): A General Framework for Computational Antibody Design," *PLoS Computational Biology* 14, no. 4 (2018): e1006112, <https://doi.org/10.1371/journal.pcbi.1006112>.
35. M. Mangoni, D. Roccatano, and A. Di Nola, "Docking of Flexible Ligands to Flexible Receptors in Solution by Molecular Dynamics Simulation," *Proteins: Structure, Function, and Bioinformatics* 35, no. 2 (1999): 153–162, [https://doi.org/10.1002/\(SICI\)1097-0134\(19990501\)35:2<153::AID-PROT2>3.0.CO;2-E](https://doi.org/10.1002/(SICI)1097-0134(19990501)35:2<153::AID-PROT2>3.0.CO;2-E).

36. V. Hornak and C. Simmerling, "Generation of Accurate Protein Loop Conformations Through Low-Barrier Molecular Dynamics," *Proteins: Structure, Function, and Bioinformatics* 51, no. 4 (2003): 577–590, <https://doi.org/10.1002/prot.10363>.
37. N. A. Ismail and S. A. Jusoh, "Molecular Docking and Molecular Dynamics Simulation Studies to Predict Flavonoid Binding on the Surface of DENV2 E Protein," *Interdisciplinary Sciences: Computational Life Sciences* 9, no. 4 (2017): 499–511, <https://doi.org/10.1007/s12539-016-0157-8>.
38. B. Dehury, V. Raina, N. Misra, and M. Suar, "Effect of Mutation on Structure, Function and Dynamics of Receptor Binding Domain of Human SARS-CoV-2 With Host Cell Receptor ACE2: A Molecular Dynamics Simulations Study," *Journal of Biomolecular Structure & Dynamics* 39, no. 18 (2021): 7231–7245, <https://doi.org/10.1080/07391102.2020.1802348>.
39. Y. Mu and G. Stock, "Conformational Dynamics of RNA-Peptide Binding: A Molecular Dynamics Simulation Study," *Biophysical Journal* 90, no. 2 (2006): 391–399, <https://doi.org/10.1529/biophysj.105.069559>.
40. B. Bertoša, B. Kojić-Prodić, R. C. Wade, and S. Tomić, "Mechanism of Auxin Interaction With Auxin Binding Protein (ABP1): A Molecular Dynamics Simulation Study," *Biophysical Journal* 94, no. 1 (2008): 27–37, <https://doi.org/10.1529/biophysj.107.109025>.
41. B. Nagarajan, S. G. Holmes, N. V. Sankaranarayanan, and U. R. Desai, "Molecular Dynamics Simulations to Understand Glycosaminoglycan Interactions in the Free- and Protein-Bound States," *Current Opinion in Structural Biology* 74 (2022): 102356, <https://doi.org/10.1016/j.sbi.2022.102356>.
42. S. Das, N. Bora, M. Ataur Rohman, R. Sharma, A. Nath Jha, and A. S. Roy, "Molecular Recognition of Bio-Active Flavonoids Quercetin and Rutin by Bovine Hemoglobin: An Overview of the Binding Mechanism, Thermodynamics and Structural Aspects Through Multi-Spectroscopic and Molecular Dynamics Simulation Studies," *Physical Chemistry Chemical Physics* 20, no. 33 (2018): 21668–21684, <https://doi.org/10.1039/C8CP02760A>.
43. Z. Payandeh, M. Rajabibazl, Y. Mortazavi, A. Rahimpour, and A. H. Taromchi, "Ofatumumab Monoclonal Antibody Affinity Maturation Through In Silico Modeling," *Iranian Biomedical Journal* 22, no. 3 (2018): 180–192, <https://doi.org/10.22034/ibj.22.3.180>.
44. L. T. Chong, Y. Duan, L. Wang, I. Massova, and P. A. Kollman, "Molecular Dynamics and Free-Energy Calculations Applied to Affinity Maturation in Antibody 4G8G7," *Proceedings of the National Academy of Sciences* 96, no. 25 (1999): 14330–14335, <https://doi.org/10.1073/pnas.96.25.14330>.
45. C. Margreitter, P. Mayrhofer, R. Kunert, and C. Oostenbrink, "Antibody Humanization by Molecular Dynamics Simulations—In-Silico Guided Selection of Critical Backmutations," *Journal of Molecular Recognition* 29, no. 6 (2016): 266–275, <https://doi.org/10.1002/jmr.2527>.
46. B. Luan and T. Huynh, "In Silico Antibody Mutagenesis for Optimizing Its Binding to Spike Protein of Severe Acute Respiratory Syndrome Coronavirus 2," *Journal of Physical Chemistry Letters* 11, no. 22 (2020): 9781–9787, <https://doi.org/10.1021/acs.jpclett.0c02706>.
47. P. Navabi, M. R. Ganjalikhany, S. Jafari, M. Dehbashi, and M. Ganjalikhani-Hakemi, "Designing and Generating a Single-Chain Fragment Variable (scFv) Antibody Against IL2R α (CD25): An In Silico and In Vitro Study," *Iranian Journal of Basic Medical Sciences* 24, no. 3 (2021): 360–368, <https://doi.org/10.22038/ijbms.2021.51709.11728>.
48. B. Wang, Z. Su, and Y. Wu, "Characterizing the Function of Domain Linkers in Regulating the Dynamics of Multi-Domain Fusion Proteins by Microsecond Molecular Dynamics Simulations and Artificial Intelligence," *Proteins* 89, no. 7 (2021): 884–895, <https://doi.org/10.1002/prot.26066>.
49. Y. Jin, L. O. Johannissen, and S. Hay, "Predicting New Protein Conformations From Molecular Dynamics Simulation Conformational Landscapes and Machine Learning," *Proteins: Structure, Function, and Bioinformatics* 89, no. 8 (2021): 915–921, <https://doi.org/10.1002/prot.26068>.
50. H. M. Berman, J. Westbrook, Z. Feng, et al., "The Protein Data Bank," *Nucleic Acids Research* 28, no. 1 (2000): 235–242, <https://doi.org/10.1093/nar/28.1.235>.
51. B. R. Brooks, R. E. Bruccoleri, B. D. Olafson, D. J. States, S. Swaminathan, and M. Karplus, "CHARMM: A Program for Macromolecular Energy, Minimization, and Dynamics Calculations," *Journal of Computational Chemistry* 4, no. 2 (1983): 187–217, <https://doi.org/10.1002/jcc.540040211>.
52. B. R. Brooks, C. L. Brooks, A. D. MacKerell, et al., "CHARMM: The Biomolecular Simulation Program," *Journal of Computational Chemistry* 30, no. 10 (2009): 1545–1614, <https://doi.org/10.1002/jcc.21287>.
53. J. V. Ribeiro, R. C. Bernardi, T. Rudack, et al., "QwikMD—Integrative Molecular Dynamics Toolkit for Novices and Experts," *Scientific Reports* 6, no. 1 (2016): 26536, <https://doi.org/10.1038/srep26536>.
54. W. Humphrey, A. Dalke, and K. Schulter, "VMD: Visual Molecular Dynamics," *Journal of Molecular Graphics* 14, no. 1 (1996): 33–38, [https://doi.org/10.1016/0263-7855\(96\)00018-5](https://doi.org/10.1016/0263-7855(96)00018-5).
55. W. L. Jorgensen, J. Chandrasekhar, J. D. Madura, R. W. Impey, and M. L. Klein, "Comparison of Simple Potential Functions for Simulating Liquid Water," *Journal of Chemical Physics* 79, no. 2 (1983): 926–935, <https://doi.org/10.1063/1.445869>.
56. A. D. MacKerell, D. Bashford, M. Bellott, et al., "All-Atom Empirical Potential for Molecular Modeling and Dynamics Studies of Proteins," *Journal of Physical Chemistry. B* 102, no. 18 (1998): 3586–3616, <https://doi.org/10.1021/jp973084f>.
57. R. B. Best, X. Zhu, J. Shim, et al., "Optimization of the Additive CHARMM All-Atom Protein Force Field Targeting Improved Sampling of the Backbone φ , ψ and Side-Chain χ_1 and χ_2 Dihedral Angles," *Journal of Chemical Theory and Computation* 8, no. 9 (2012): 3257–3273, <https://doi.org/10.1021/ct300400x>.
58. J. C. Phillips, D. J. Hardy, J. D. C. Maia, et al., "Scalable Molecular Dynamics on CPU and GPU Architectures With NAMD," *Journal of Chemical Physics* 153, no. 4 (2020): 44130, <https://doi.org/10.1063/5.0014475>.
59. G. J. Martyna, D. J. Tobias, and M. L. Klein, "Constant Pressure Molecular Dynamics Algorithms," *Journal of Chemical Physics* 101, no. 5 (1994): 4177–4189, <https://doi.org/10.1063/1.467468>.
60. S. E. Feller, Y. Zhang, R. W. Pastor, and B. R. Brooks, "Constant Pressure Molecular Dynamics Simulation: The Langevin Piston Method," *Journal of Chemical Physics* 103, no. 11 (1995): 4613–4621, <https://doi.org/10.1063/1.470648>.
61. W. Kabsch, "A Solution for the Best Rotation to Relate Two Sets of Vectors," *Acta Crystallogr. Sect. A* 32, no. 5 (1976): 922–923, <https://doi.org/10.1107/S0567739476001873>.
62. W. Kabsch, "A Discussion of the Solution for the Best Rotation to Relate Two Sets of Vectors," *Acta Crystallogr. Sect. A* 34, no. 5 (1978): 827–828, <https://doi.org/10.1107/S0567739478001680>.
63. A. Leaver-Fay, M. Tyka, S. M. Lewis, et al., "ROSETTA3: An Object-Oriented Software Suite for the Simulation and Design of Macromolecules," *Methods in Enzymology* 487 (2011): 545–574, <https://doi.org/10.1016/B978-0-12-381270-4.00019-6>.
64. C. Roy and S. Datta, "ASBAAC: Automated Salt-Bridge and Aromatic-Aromatic Calculator," *Bioinformation* 14, no. 4 (2018): 164–166, <https://doi.org/10.6026/97320630014164>.
65. P. A. Wood, F. H. Allen, and E. Pidcock, "Hydrogen-Bond Directionality at the Donor H Atom—Analysis of Interaction Energies

- and Database Statistics," *CrystEngComm* 11, no. 8 (2009): 1563–1571, <https://doi.org/10.1039/B902330E>.
66. M. Cohen, D. Reichmann, H. Neuvirth, and G. Schreiber, "Similar Chemistry, but Different Bond Preferences in Inter Versus Intra-Protein Interactions," *Proteins: Structure, Function, and Bioinformatics* 72, no. 2 (2008): 741–753, <https://doi.org/10.1002/prot.21960>.
67. V. Kunik, B. Peters, and Y. Ofran, "Structural Consensus Among Antibodies Defines the Antigen Binding Site," *PLoS Computational Biology* 8, no. 2 (2012): e1002388, <https://doi.org/10.1371/journal.pcbi.1002388>.
68. R. F. Alford, A. Leaver-Fay, J. R. Jeliazkov, et al., "The Rosetta All-Atom Energy Function for Macromolecular Modeling and Design," *Journal of Chemical Theory and Computation* 13, no. 6 (2017): 3031–3048, <https://doi.org/10.1021/acs.jctc.7b00125>.
69. H. B. Mann and D. R. Whitney, "On a Test of Whether One of Two Random Variables Is Stochastically Larger Than the Other," *Annals of Mathematical Statistics* 18, no. 1 (1947): 50–60.
70. P. Virtanen, R. Gommers, T. E. Oliphant, et al., "SciPy 1.0: Fundamental Algorithms for Scientific Computing in Python," *Nature Methods* 17, no. 3 (2020): 261–272, <https://doi.org/10.1038/s41592-019-0686-2>.
71. R. L. Dunbrack, Jr. and F. E. Cohen, "Bayesian Statistical Analysis of Protein Side-Chain Rotamer Preferences," *Protein Science* 6, no. 8 (1997): 1661–1681, <https://doi.org/10.1002/pro.5560060807>.
72. D. Kozakov, D. R. Hall, B. Xia, et al., "The ClusPro Web Server for Protein–Protein Docking," *Nature Protocols* 12, no. 2 (2017): 255–278, <https://doi.org/10.1038/nprot.2016.169>.
73. C. Dominguez, R. Boelens, and A. M. J. J. Bonvin, "HADDOCK: A Protein–Protein Docking Approach Based on Biochemical or Biophysical Information," *Journal of the American Chemical Society* 125, no. 7 (2003): 1731–1737, <https://doi.org/10.1021/ja026939x>.
74. S. Lyskov and J. J. Gray, "The RosettaDock Server for Local Protein–Protein Docking," *Nucleic Acids Research* 36, no. Web Server (2008): W233–W238, <https://doi.org/10.1093/nar/gkn216>.
75. B. G. Pierce, K. Wiehe, H. Hwang, B.-H. Kim, T. Vreven, and Z. Weng, "ZDOCK Server: Interactive Docking Prediction of Protein–Protein Complexes and Symmetric Multimers," *Bioinformatics* 30, no. 12 (2014): 1771–1773, <https://doi.org/10.1093/bioinformatics/btu097>.
76. S. Basu and B. Wallner, "DockQ: A Quality Measure for Protein–Protein Docking Models," *PLoS One* 11, no. 8 (2016): e0161879, <https://doi.org/10.1371/journal.pone.0161879>.
77. F. Pedregosa, G. Varoquaux, A. Gramfort, et al., "Scikit-Learn: Machine Learning in Python," *Journal of Machine Learning Research* 12, no. 85 (2011): 2825–2830.
78. M. F. Lensink, R. Méndez, and S. J. Wodak, "Docking and Scoring Protein Complexes: CAPRI 3rd Edition," *Proteins: Structure, Function, and Bioinformatics* 69, no. 4 (2007): 704–718, <https://doi.org/10.1002/prot.21804>.

Supporting Information

Additional supporting information can be found online in the Supporting Information section.